Magnesium Technology 2012
Edited by: Suveen N. Mathaudhu, Wim H. Sillekens, Neale R. Neelameggham, and Norbert Hort
TMS (The Minerals, Metals & Materials Society), 2012

THE EFFECTS OF STRAIN AND STRESS STATE IN HOT FORMING OF MG AZ31 SHEET

Paul A. Sherek[1], Alexander J. Carpenter[1], Louis G. Hector, Jr.[2], Paul E. Krajewski[2], Jon T. Carter[2], Joshua Lasceski[2], and Eric M. Taleff[1]
[1]The University of Texas at Austin; Department of Mechanical Engineering; 1 University Station C2200; Austin, TX 78712-0292, USA
[2]General Motors Corp.; Research and Development; MC 480-106-212; 30500 Mound Rd.; Warren, MI 48090-9055, USA

Keywords: AZ31, bulge forming, material constitutive model

Abstract

Wrought magnesium alloys, such as AZ31 sheet, are of considerable interest for light-weighting of vehicle structural components. The poor room-temperature ductility of AZ31 sheet has been a hindrance to forming the complex part shapes necessary for practical applications. However, the outstanding formability of AZ31 sheet at elevated temperature provides an opportunity to overcome that problem. Complex demonstration components have already been produced at 450°C using gas-pressure forming. Accurate simulations of such hot, gas-pressure forming will be required for the design and optimization exercises necessary if this technology is to be implemented commercially. We report on experiments and simulations used to construct the accurate material constitutive models necessary for finite-element-method simulations. In particular, the effects of strain and stress state on plastic deformation of AZ31 sheet at 450°C are considered in material constitutive model development. Material models are validated against data from simple forming experiments.

Introduction

In the automotive and aircraft industries, weight reduction is an effective method of increasing both the fuel efficiency and performance of a vehicle [1-3]. For this reason, lightweight structural materials, such as magnesium alloys, are often preferred over heavier materials. Magnesium is attractive because of its low density, compared to steel or aluminum [4-6]. Because of its low density, a magnesium component can be designed with less weight than a corresponding steel or aluminum component with the same bending strength and stiffness [7]. However, magnesium alloys typically possess poor ductility at room temperature [8]. To obtain sufficient ductility for forming complex parts, high-temperature forming operations, such as superplastic forming (SPF) and quick plastic forming (QPF), can be used [9, 10]. In both SPF and QPF, a sheet metal blank is clamped between two dies and gas-pressure is applied to form the sheet into a die cavity. Such technologies have been used to produce demonstration automotive panels from Magnesium alloy AZ31 sheet [11].

Finite-element-method (FEM) simulations can assist in determining the processing parameters (gas-pressure, temperature, etc.) necessary for gas-pressure forming of complex components. For FEM simulations, the deformation response of a workpiece material is described mathematically through a constitutive model that relates strain to stress. Thus, FEM simulation results are only accurate if an accurate constitutive model is used. Constitutive models describing material deformation behaviors at elevated temperatures are most commonly developed using data from tensile tests [12, 13]. However, data from gas-pressure, bulge-forming experiments at elevated temperature have also been used to inform constitutive models [14-16].

The high-temperature deformation behavior of magnesium sheet materials has most frequently been described in the literature with single-term material constitutive models [12-16], which are designed to predict forming behavior when only one deformation mechanism is active, such as grain-boundary-sliding (GBS) creep. A previous study determined that two-term material constitutive models can be more accurate than single-term models when deformation is controlled by two active deformation mechanisms in an aluminum alloy, which is commonly the case in SPF and QPF operations [17]. A two-term material constitutive model was developed using strain-rate-change (SRC) tensile tests of fine-grained AZ31 at temperatures from 300 to 500°C and strain rates from 10^{-4} to 3×10^{-2} s^{-1} [18]. The constitutive equation used is,

$$\dot{\varepsilon} = A_1\left(\frac{\sigma}{E}\right)^{n1}\exp\left(\frac{-Q_1}{RT}\right) + A_2\left(\frac{\sigma}{E}\right)^{n2}\exp\left(\frac{-Q_2}{RT}\right), \quad (1)$$

where $\dot{\varepsilon}$ is the true-strain rate, A is a material constant, n is the stress exponent, σ is the true flow stress, E is the Young's modulus, and Q is the activation energy for creep. The subscripts 1 and 2 denote GBS and dislocation-climb creep terms respectively, which are the deformation mechanisms potentially active over the range of conditions investigated. A constitutive model in the form of Equation (1) was derived from tensile data [18]. While it provided accurate predictions of behavior under uniaxial tension, it was far less accurate in predicting deformation under biaxial tension, as determined by comparing predictions to data from gas-pressure bulge tests. A second model was created to improve the agreement of FEM simulation predictions with data from bulge forming experiments. This second model, the "1.3 σ" model, reduces the effective stress in the dislocation-climb creep term of Equation (1) by dividing the flow stress in the second term by 1.3. Simulation predictions using the 1.3 σ model reasonably predict pole heights from gas-pressure bulge tests at 450°C for a range of pressures. The 1.3 σ model, however, does not account for significant hardening in the AZ31 material at slow strain rates [18].

The purpose of the present study is to construct new two-term strain-dependent material constitutive models from AZ31 tensile data at 450°C. These new constitutive material models are used in FEM simulations, the predictions of which are compared to the results of simulations using the older models at 450°C and to data from both tensile tests and gas-pressure bulge forming experiments.

Material Constitutive Model Creation

Tensile Tests

Material constitutive models were created using data from tensile tests of AZ31 sheet at 450°C. The sheet composition is provided

in Table I. Dog-bone shaped tensile coupons with a gauge length of 25 mm, gauge width of 6 mm, and a shoulder radius of 3 mm were machined from sheet with an as-received thickness of 2 mm. The tensile axis of coupons was oriented at 0°, 45°, or 90° relative to the rolling direction. Each coupon was pulled in tension to a true strain of 0.6 at 450°C and a constant true-strain rate in the range of 10^{-4} to 10^{-1} s^{-1}. Testing followed the procedures described in ASTM E 2448-06 [19]. Load and cross-head extension were measured as functions of time during each test and were used to calculate true stress and true strain. The stress-strain data were corrected for machine stiffness by enforcing the elastic modulus of pure Magnesium at 450°C, 32 GPa [20].

Table I. Composition of the AZ31 sheet material in wt. pct.

Al	Zn	Mn	Fe	Cu	Ni
3.1	1.0	0.42	0.006	0.003	<0.003
Si	**Ca**	**Be**	**Sr**	**Ce**	**Mg**
<0.1	<0.01	<0.005	<0.005	<0.01	Bal.

Analysis of Tensile Data

At strain rates from 10^{-4} to 3×10^{-3} s^{-1}, flow stress increases with true strain. The Voce strain-hardening law

$$\sigma = \sigma_o + a\left(1 - \exp\left(-c\varepsilon\right)\right) \tag{2}$$

was fit to these data, where σ is flow stress, σ_o is initial yield strength, a and c are fitting parameters, and ε is true strain. Flow stress is approximately constant with strain for strain rates from 10^{-2} to 10^{-1} s^{-1}, and only a mean flow stress, σ_m, was calculated for these conditions. The Voce law parameters and average flow stresses calculated during fitting are presented in Table II. The values in Table II indicate that specimen orientation has little effect on flow stress for a given strain rate. Thus, subsequent analyses assumed flow stress to be the average of all three orientations.

Table II. Parameters for the Voce law and the mean flow stress

Strain rate, s^{-1}	Orientation, degrees	σ_o, MPa	a, MPa	c	σ_m, MPa
10^{-4}	0	1.73	8.02	1.96	-
	45	1.77	6.85	2.15	-
	90	1.81	6.68	2.42	-
3×10^{-4}	0	4.01	6.65	3.23	-
	45	3.89	6.72	3.40	-
	90	4.18	6.36	3.83	-
10^{-3}	0	8.78	4.72	4.41	-
	45	8.79	4.73	4.56	-
	90	8.90	4.63	4.83	-
3×10^{-3}	0	14.2	2.05	6.34	-
	45	14.2	2.21	5.95	-
	90	14.7	1.72	7.11	-
10^{-2}	0	19.8	-	-	20.0
	45	20.0	-	-	20.3
	90	20.4	-	-	20.6
3×10^{-2}	0	24.0	-	-	24.6
	45	24.2	-	-	24.7
	90	24.7	-	-	25.1
10^{-1}	0	28.7	-	-	30.1
	45	29.0	-	-	30.4
	90	29.2	-	-	30.5

The fitted parameters in Table II were used to calculate flow stress for each test strain rate at strains from 0 to 0.6, in increments of 0.1. These calculated data are shown in Figure 1. At each strain, the following phenomenological equation for creep deformation was fit to the data,

$$\dot{\varepsilon} = A_1\sigma_1^{n1} + A_2\sigma_2^{n2} \tag{3}$$

where $\dot{\varepsilon}$ is true-strain rate, A and n are fitting parameters, and σ is true stress. This equation represents the effect of two independent creep deformation mechanisms. Mechanism 1 (first term) governs deformation at the slowest rates, while mechanism 2 (second term) governs deformation at the fastest rates. These are the GBS and dislocation-climb creep mechanisms, respectively, previously discussed.

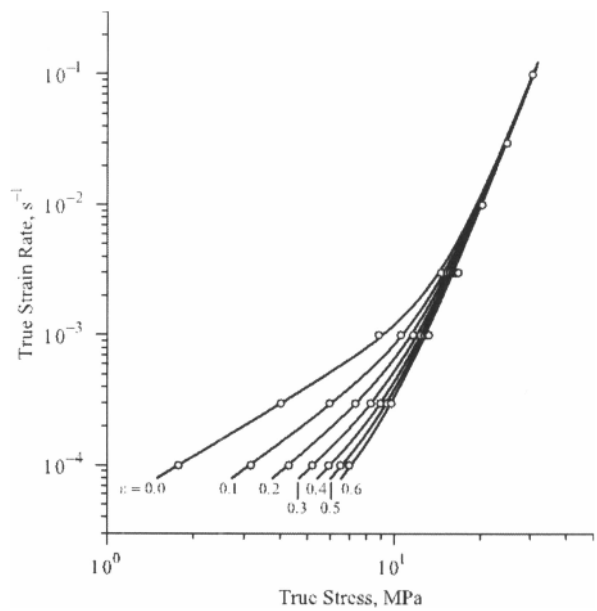

Figure 1. The logarithm of true-strain rate is plotted against the logarithm of true stress for AZ31 tensile data at strains from 0 to 0.6. All specimens were tested at 450°C. Curves represent fits of Equation (3) to the calculated data.

The fits in Figure 1 produced values of A_2 and n_2 which are constant with strain

$$A_2 = 5.90\times10^{-10}\ s^{-1}\ MPa^{-n2} \tag{4}$$

$$n2 = 5.54 \tag{5}$$

This value of $n2$ suggests that dislocation-climb creep is the active mechanism at the fastest strain rates [22]. However, A_1 and $n1$ were observed to vary significantly with strain. The fitted values of $n1$ vary between 1.333 and 2, and are described reasonably by,

$$n1(\varepsilon) = 1.333 + 0.667\tanh\left(4.63\varepsilon\right) \tag{6}$$

Assuming these values for $n1$, the following equation was fit to A_1, with units of s^{-1} MPa^{-n1}, as a function of true strain,

$$A_1(\varepsilon) = \exp\left(-9.98 - 12.59\varepsilon + 17.85\varepsilon^2 - 11.10\varepsilon^3\right) \quad (7)$$

The range of values observed for $n1$ suggests that GBS creep is the active mechanism at the slowest strain rates [22]. The material model described by Equations (3) through (7) is designated the strain-dependent tensile data (SDTD) material model.

After comparison with data from bulge forming experiments, the effective flow stress in the dislocation-climb creep term, the second term of Equation (2), was reduced. This was accomplished by dividing the flow stress in this term only by 1.3, as was previously done for the 1.3 σ model [18]. This produced a new value of A_2,

$$A_2 = 1.38 \times 10^{-10}\ \text{s}^{-1}\ \text{MPa}^{-n2} \quad (8)$$

The model described using Equation (3) with Equations (5) through (8) is designated the SDTDM1 (SDTD modification #1) model.

Model Validation Procedure

Gas-Pressure Bulge Forming Experiments

Gas-pressure bulge forming experiments were performed using a custom apparatus described in Ref. [23]. For these experiments, specimen blanks machined from AZ31 sheet were formed at 450°C using gas pressure. The blanks are disks with a diameter of 90.2 mm and the as-received sheet thickness of 2 mm. A schematic of the experiment is shown in Figure 2. During each experiment, an AZ31 blank was placed between two die halves. The lower die half has a cylindrical cavity with an inner diameter of D_{cavity} = 55.4 mm, a sealing bead diameter of D_{bead} = 64.8 mm, and a die-entry radius of 1.5 mm, see Figure 2. Forming began after the blank reached 450°C, as measured by a thermocouple placed adjacent to the blank. Normal preheat times to reach and stabilize at the test temperature varied from 20 to 60 minutes. In selected short-preheating experiments, the blank was preheated for only 5 minutes prior to forming. Upon the completion of preheating, gas-pressure was applied to the top of the blank, causing it to form downward into a bulge shape similar to an inverted dome. A balanced biaxial stress state occurs at the dome peak during forming. The pressures applied ranged from 500 to 1240 kPa. Dome pole displacement was measured *in situ* during deformation using a digital micrometer with a remote-contact gauge assembly.

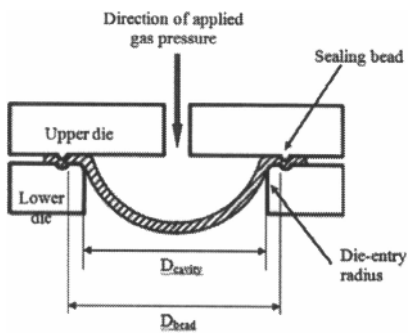

Figure 2. The bulge forming experiment is shown [23].

Finite Element Method Simulations

Tensile test experiments of AZ31 sheet material were simulated using the FEM software package Abaqus™ 6.8 [24]. The gauge section of a tensile coupon 25 mm long, 6 mm wide, and 2 mm thick was meshed using quadrilateral elements. One end of the mesh was held fixed in the tensile direction, while the other end was displaced along the tensile direction to reproduce the constant true-strain rate of the tensile test. Tensile simulations were conducted using the SDTD and SDTDM1 material models.

Bulge forming tests of AZ31 sheet were simulated using Abaqus™ 6.8. The AZ31 blank mesh consisted of a circle with diameter 64.8 mm, which is the diameter of the sealing bead used in experiments. The die mesh had the same diameter and entry radius used in forming experiments. Both the blank and die were modeled using quadrilateral membrane elements. The mesh sensitivity of a similar geometry was previously investigated, and the used here mesh was shown to be sufficient [17]. Bulge simulations used the 1.3 σ, SDTD, and SDTDM1 material models.

Results

Uniaxial Tension

The stress-strain curves from tensile simulations are presented with experimental data from tensile tests in Figures 3(a) and (b) for true-strain rates of 10^{-4} and 10^{-1} s^{-1}, respectively. At the slowest rate of 10^{-4} s^{-1}, there is substantial strain hardening in uniaxial tension. The SDTD model accurately predicts these stress-strain data. The SDTDM1 model agrees well with experimental data up to a strain of approximately 0.4, but it predicts a slightly higher flow stress beyond this strain. The only difference between the SDTD and SDTDM1 models is the dislocation-climb creep term. This further confirms that the governing creep mechanism at this rate is primarily grain-boundary sliding. At 10^{-1} s^{-1}, almost no strain hardening is observed in the tensile data, and deformation occurs almost entirely by dislocation-climb creep at this fast rate. The SDTD model accurately predicts tensile data at this strain rate, while the SDTDM1 model predicts much higher flow stresses than observed experimentally. This relative accuracy between the two models will later be contrasted against predictions for bulge tests. Predictions and test data at intermediate strain rates reveal a gradual transitions between the behaviors exhibited in Figures 3(a) and (b).

Biaxial Bulge Forming

Figures 4(a) through (c) show bulge pole height as a function of time from gas-pressure bulge forming experiments (normal preheat) for gas pressures of 550, 830, and 1100 kPa, respectively. For each pressure, experimental data are compared with FEM simulation results using the 1.3 σ, SDTD, and SDTDM1 models. Note that results from two experiments, each represented by a separate curve, are shown for each test condition. At 550 kPa, both the SDTD and SDTDM1 models provide similar predictions of bulge height. The two models predict slightly larger bulge heights than observed experimentally. The 1.3 σ model, which contains no strain-dependent term, predicts significantly faster forming than observed experimentally. These results confirm that strain hardening must be accounted for to accurately predict

forming at slow forming rates. At 830 kPa, the SDTD model predicts faster forming than the 1.3 σ model, and both models predict faster forming than observed experimentally. The SDTDM1 model provides the most accurate predictions of bulge heights at this pressure. At 1100 kPa, the accuracy of the 1.3 σ model increases to provide predictions similar to the SDTDM1 model, while the SDTD model continues to predict much larger dome heights than observed experimentally. These results suggest that the reduction in effective flow stress in *only* the dislocation-climb creep term, i.e., the 1.3 σ correction factor, is necessary to accurately predict deformation under a biaxial stress state.

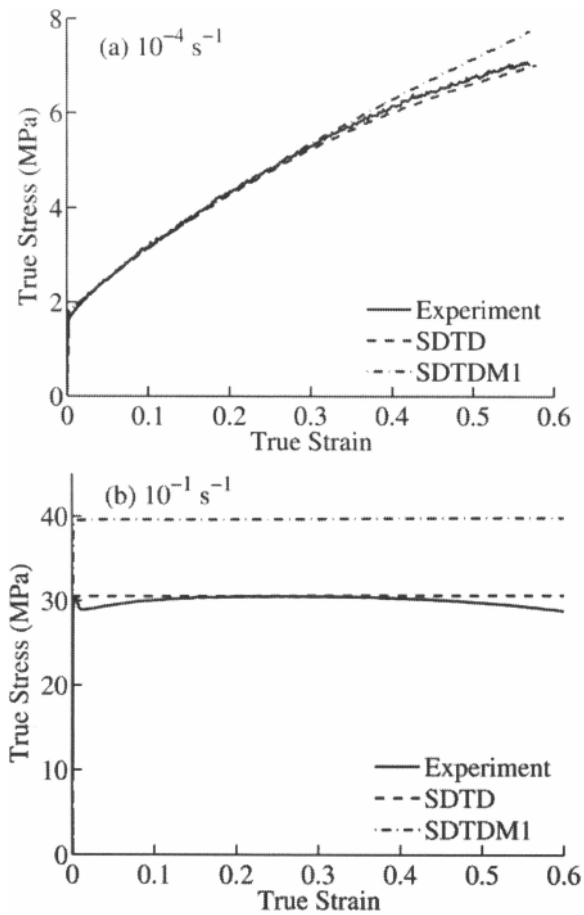

Figure 3. Stress-strain curves are shown for tensile data and simulations at 450°C and strain rates of (a) 10^{-4} and (b) 10^{-1} s^{-1}.

Short-preheat bulge forming experimental data are compared with normal-preheat data and SDTDM1 simulation results in Figures 5(a) through (c) for pressures of 550, 830, and 1100 kPa, respectively. The short-preheat experiments were designed to determine if there is any effect of preheating time on forming, such as might occur if static grain growth during preheating slowed GBS creep. Note that results from two long-preheat experiments, each represented by a separate curve, are shown for each test condition. At 550 kPa, the material forms more rapidly during the short preheat experiment than during the normal-preheat experiment, though forming is still slower than predicted by the SDTDM1 model. At 830 kPa, the SDTDM1 model results more closely match the short preheat data than the normal preheat data. At 1100 kPa, there is little difference between short-preheat and normal-preheat data. These results indicate that the material hardens slightly during preheating, but this effect slows only deformation attributable to GBS creep.

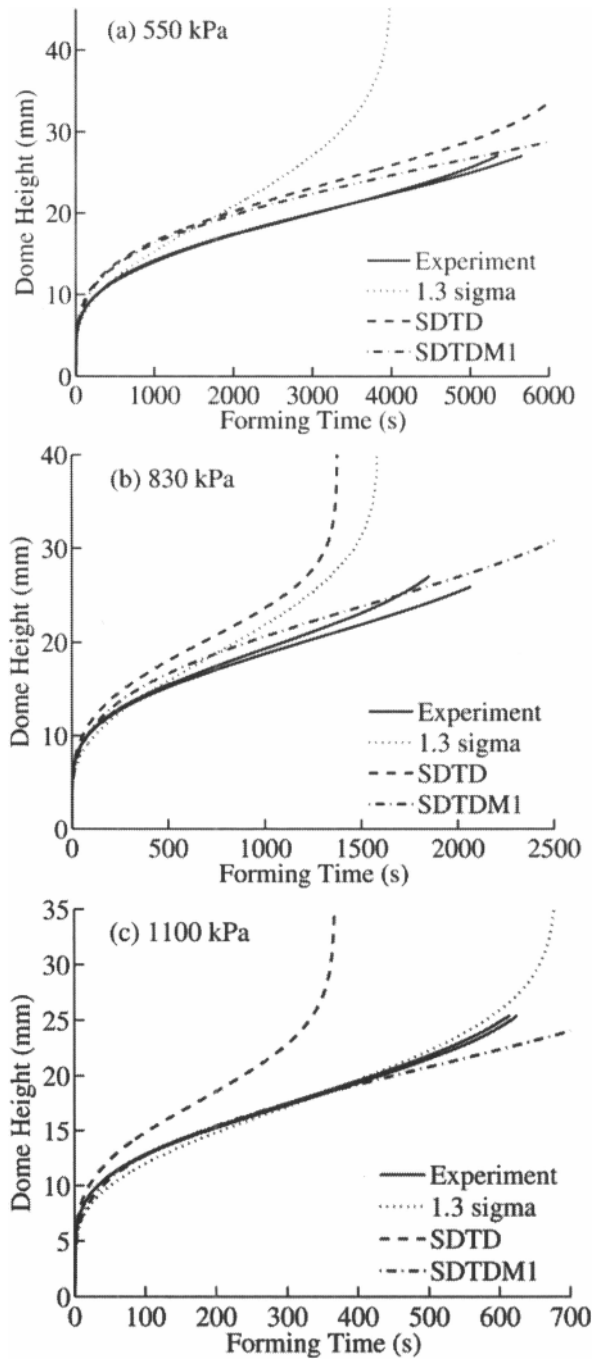

Figure 4. Bulge pole height is plotted against forming time for bulge forming experiments and simulations at 450°C and gas-pressures of (a) 550, (b) 830, and (c) 1100 kPa.

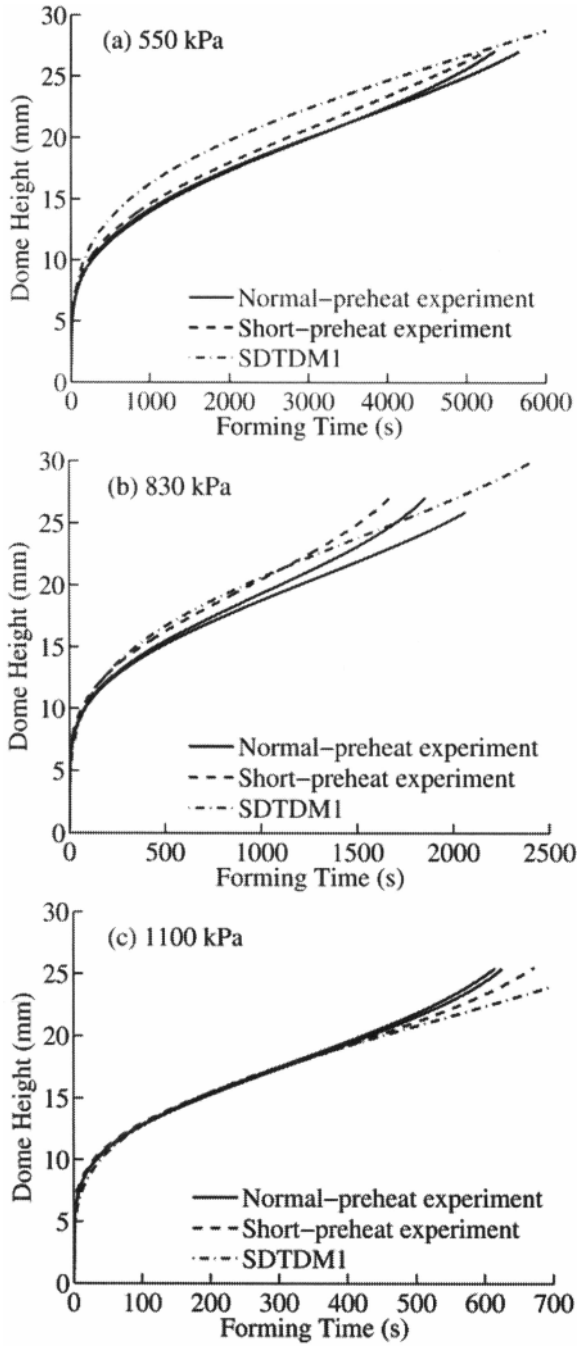

Figure 5. Bulge pole height is plotted against forming time for SDTDM1 simulations and experiments using both a normal preheat and a short preheat at 450°C and gas-pressures of (a) 550, (b) 830, and (c) 1100 kPa. Normal preheat times generally varied between 20 and 60 minutes, while short preheating was 5 minutes.

Discussion

Tensile test data at the slowest strain rate of 10^{-4}, see Figure 3, exhibit significant strain hardening. At the fastest strain rate of 10^{-1} s^{-1}, flow stress is approximately constant with strain. These results indicate that strain hardening only occurs during GBS creep, which controls deformation at slow strain rates. At fast strain rates, dislocation-climb creep dominates and no strain hardening is observed. A two-term material constitutive model with a strain-dependent GBS creep term can account for this behavior. For bulge forming at 550 kPa, the lowest pressure examined, simulations based on either strain-dependent material models, SDTD or SDTDM1, are in better agreement with bulge data than simulations using the 1.3 σ model, which contains no strain dependence. Accounting for strain hardening is required to accurately predict AZ31 forming behavior at the slow strain rates for which GBS creep dominates. However, the results of bulge forming experiments and simulations at 830 and 1100 kPa show that the SDTD model is less accurate than the 1.3 σ and SDTDM1 models at these pressures. The effective stress for dislocation-climb creep flow stress is reduced in both the 1.3 σ and SDTDM1 models, but not the SDTD model. This indicates that a reduction in effective flow stress for dislocation-climb creep, through the 1.3 correction factor, is required to accurately predict biaxial forming of AZ31 at the fast strain rates for which dislocation-climb creep dominates.

Strain hardening at slow strain rates may be explained by dynamic grain growth. At constant temperature, GBS creep is dependent on grain size in the following manner,

$$\dot{\varepsilon} = \frac{A}{d^p}\sigma^n \tag{9}$$

where $\dot{\varepsilon}$ is strain rate, A is a material constant, d is grain size, p is the grain-size exponent, σ is stress, and n is the stress exponent [22]. As grain size increases, flow stress must also increase to maintain a constant true-strain rate. Thus, the strain-hardening term in the SDTD and SDTDM1 models might be interpreted as a method to account for grain growth during deformation. Similarly, static grain growth may explain the differences between experimental data from normal-preheat and short-preheat bulge tests, shown in Figure 5. As preheat time prior to deformation increases, grain size is expected to increase from static grain growth. In this way, the normal-preheat specimens will have a larger initial grain size than the short-preheat specimens at the onset of deformation, which manifests as a slower forming rate when GBS creep controls deformation. This behavior is observed at forming pressures of 550 and 830 kPa, which is consistent with GBS creep dominating. There is no significant difference in forming rates between normal-preheat and short-preheat specimens at the highest pressure, 1100 kPa. This is consistent with deformation by dislocation-climb creep at the highest pressure. Grain size has no effect on dislocation-climb creep [22] at the fast strain rates associated with the highest test pressure.

The SDTD model consistently provides better predictions of deformation under uniaxial tension than does the SDTDM1 model, see Figure 3. However, the SDTDM1 model consistently provides better predictions of deformation under biaxial tension than does the SDTD model, see Figure 4. This result indicates a

fundamentally important effect of stress state on dislocation-climb creep for the AZ31 sheet material at 450°C. The rate of dislocation-climb creep is slower under balanced-biaxial tension than under uniaxial tension, and this difference requires an artificial reduction in the effective stress for dislocation-climb creep by the 1.3 factor used in the SDTDM1 model. The reason for this effect of stress state on dislocation-climb creep is not clear. In a previous study of hot deformation in aluminum alloy AA5083, an effect of stress state was observed for GBS creep only, such that increasing hydrostatic stress increased the creep rate [17]. However, no effect of stress state is observed for GBS creep in the AZ31 material. Thus, the case of AZ31 is unique. One possible source for the effect of stress state on dislocation-climb creep in AZ31 is plastic anisotropy arising from crystallographic texture. The crystal structure of magnesium is HCP, which produces a limited number of slip systems, even at elevated temperatures. Indeed, it is the activation of additional slip systems with increasing temperature that causes significant ductility increases for AZ31 as temperature increases. A strong initial crystallographic texture, in conjunction with a limited number of potential slip systems, could easily lead to plastic anisotropy in dislocation-climb creep. Such plastic anisotropy could readily produce differences between deformation under uniaxial and biaxial tension. The possibility of normal plastic anisotropy, such as might arise out of the basal textures common in rolled magnesium sheet materials, would be worthy of further investigation; normal anisotropy is still consistent with the isotropic in-plane flow stresses reported in Table II. Plastic anisotropy would be expected to affect dislocation-climb creep, which proceeds by the usual slip processes, but not GBS creep. GBS creep involves relative sliding and rotation of grains, which makes it less susceptible to plastic anisotropy and can also lead to randomization of crystallographic texture [25, 26].

Conclusions

Two strain-dependent material constitutive models, the SDTD and SDTDM1 models, were developed to account for the effects of strain and stress state on the deformation of AZ31 sheet at 450°C. AZ31 sheet material was tested under uniaxial tension at constant true-strain rates from 10^{-4} to 10^{-1} s^{-1}, and the SDTD material model was constructed from these tensile data. Comparisons between FEM simulations and 450°C gas-pressure bulge test data were used to construct the SDTDM1 model, which accounts for the effect of stress state on dislocation-climb creep. At slow strain rates, significant strain hardening occurs during tensile deformation, which is accounted for by a strain-dependent GBS creep term. This strain-dependent term is required to accurately predict biaxial bulge forming behavior at low forming pressures, for which GBS creep dominates deformation. The observed strain hardening during GBS creep is likely a product of dynamic grain growth. Static grain growth qualitatively explains the observed decrease in forming rate with increasing preheat time. Experimental data indicate a difference in the flow stress for dislocation-climb creep between uniaxial and biaxial tension. This effect of biaxial tension is accounted for in the SDTDM1 model by reducing the effective stress in only the dislocation-climb creep term through division of stress by a 1.3 factor. It is proposed that this effect of stress state is the result of plastic anisotropy resulting from crystallographic texture, but this proposition has not yet been explored.

References

1. L.H. Pomeroy: *Automotive Engineering*, 1922, vol. XI, no. 6, pp. 508-19.
2. G.S. Cole, A.M. Sherman: *Mater. Char.*, 1995, vol. 35, pp. 3-9.
3. J.J. Lee, S.P. Lukachko, I.A. Waitz, A. Schafer: Annual Review of Energy and the Environment, 2001, vol. 26, pp. 167-200.
4. D. Eliezer, E. Aghion, F.H. Froes: *Adv. Perform Mater.*, 1998, vol. 5, pp. 201-12.
5. M.M. Avedesian, H. Baker: *Magnesium and Magnesium Alloys*, ASM International, Materials Park, OH, 1999, pg. iv.
6. B.L. Mordike, T. Ebert: *Mater. Sci. Eng. A*, 2001, vol. 302, pp. 37-45.
7. A.A. Luo: *JOM*, 2002, vol. 54, no. 2, pp. 42-48.
8. M.W. Toaz, E.J. Ripling: *J. Met.*, 1956, vol. 8, pp. 936-46.
9. J.G. Schroth: in Advances in Superplasticity and Superplastic Forming, E.M. Taleff, P.A. Friedman, P.E. Krajewski, R.S. Mishra, and J.G. Schroth, eds., TMS, Warrendale, PA, 2004, pp. 9-20.
10. P.E. Krajewski, J.G. Schroth: *Mat. Sci. Forum*, 2007, vol. 551-552, pp. 3-12.
11. R. Verma, L.G. Hector, Jr., P.E. Krajewski, E.M. Taleff: *JOM*, 2009, vol. 61, no. 8, pp. 29-37.
12. M.K. Khraisheh, F.K. Abu-Farha, M.A. Nazzal, K.J. Weinmann: *Annals of CIRP*, 2006, vol. 55, pp. 233.
13. F.K. Abu-Farha, M.K. Khraisheh: *Adv. Eng. Mater.*, 2007, vol. 9, pp. 777-83.
14. G. Palumbo, D. Sorgente, L. Tricarico, S.H. Zhang, W.T. Zheng, L.X. Zhou, L.M. Ren: *Mat. Sci. Forum*, 2007, vol. 551-552, pp. 317-22.
15. G. Giuliano, S. Franchitti: *Int. J. Mach. Tool Manu.*, 2008, vol. 48, pp. 1519-1522.
16. A.-W. El-Morsy, K. Manabe, H. Nishimura: *Mater. Trans.*, 2002, vol. 43, pp. 2443-48.
17. E.M. Taleff, L.G. Hector, Jr., J.R. Bradley, R. Verma, P.E. Krajewski: *Acta Mater.*, 2009, vol. 57, pp. 2812-22.
18. E.M. Taleff, L.G. Hector, Jr., R. Verma, P.E. Krajewski, J.-K. Chang: *J. Mater. Eng. Perform.*, 2010, vol. 19, pp. 488-94.
19. ASTM E 2448-06. *Standard Test Method for Determining the Superplastic Properties of Metallic Sheet Materials*. ASTM: West Conshohocken, PA. (2006).
20. W. Köster: *Z. Metallkd.*, 1948, vol. 39, pp. 1-9.
21. ASTM E 112-96. *Standard Test Methods for Determining Average Grain Size*. ASTM: West Conshohocken, PA. (1996).
22. O.D. Sherby and P.M. Burke: *Progr. Mater. Sci.*, 1968, vol. 13, pp. 325-90.
23. R.V. Moller: "Design and Fabrication of an Instrument to Test the Mechanical Behavior of Aluminum Alloy Sheets During High-Temperature Gas-Pressure Blow Forming," Thesis, Mechanical Engineering, The University of Texas at Austin, 2008.
24. Dassault Systèmes Simulia Corp., Abaqus (Version 6.8), Providence, RI.
25. T.E. Langdon : *J. Mater. Sci.*, 2009, vol. 44, pp. 5998-6010.
26. M.T. Pèrez-Prado, G. González-Doncel, O.A. Ruano and T.R. McNelley: *Acta Mater.*, 2001, vol. 49, pp. 2259-2268.